PHYSICAL REVIEW B **93**, 155155 (2016)

Band flatness optimization through complex analysis

Ching Hua Lee,[1,*] Daniel P. Arovas,[2] and Ronny Thomale[3]

[1] *Institute of High Performance Computing, 138632, Singapore*

[2] *Department of Physics, University of California at San Diego, La Jolla, California 92093, USA*

[3] *Institute for Theoretical Physics, University of Würzburg, Am Hubland, 97074 Würzburg, Germany*

(Received 16 November 2015; published 26 April 2016)

Narrow-band electron systems are particularly likely to exhibit correlated many-body phases driven by interaction effects. Examples include magnetic materials, heavy-fermion systems, and topological phases such as fractional quantum Hall states and their lattice-based cousins, the fractional Chern insulators (FCIs). Here we discuss the problem of designing models with optimal band flatness, subject to constraints on the range of electron hopping. In particular, we show how the *imaginary gap*, which serves as a proxy for band flatness, can be optimized by appealing to Rouché's theorem, a familiar result from complex analysis. This leads to an explicit construction which we illustrate through its application to two-band FCI models with nontrivial topology (i.e., nonzero Chern numbers). We show how the imaginary-gap perspective leads to an elegant geometric picture of how topological properties can obstruct band flatness in systems with finite-range hopping.

DOI: 10.1103/PhysRevB.93.155155

I. INTRODUCTION

The accumulation of electronic energy states in narrow-band systems often results in interaction-driven strongly correlated many-body phases. The limiting case in which one or more narrow bands become perfectly flat has attracted recent attention in both condensed-matter and cold-atom physics [1,2], with several proposals for realization with realistic materials [3–8]. Unlike van Hove singularities [9] and other prominences which can lead to nesting instabilities, flatbands are featureless in momentum space and thus tend to support similarly featureless many-body states, i.e., without breaking of lattice symmetries. A classic example is the Stoner instability leading to ferromagnetism, which is rigorously established for flatband systems [10,11], but notoriously difficult to elicit with typically dispersing bands. In systems with attractive effective interactions, flatbands and related density profiles tend to favor a featureless s-wave superconductor [12,13] over competing charge density wave states. Correlated states where discrete lattice symmetries are spontaneously broken by interaction are also possible in flatband systems, especially at low filling [14]. In addition to broken-symmetry states, topological states known as fractional Chern insulators (FCIs) [15–20] have been identified in interacting nearly-flatband models. These systems are lattice realizations of the fractional quantum Hall effect, where their nearly flatbands effectively serve as Landau levels.

Besides the atomic limit with trivially dispersionless bands, flatbands can also arise in noninteracting systems [21]. Tasaki [1] has described both long-range hopping as well as local "cell construction" models yielding flatbands which rigorously exhibit ferromagnetism when Hubbard interactions are included. The class of lattices known as *line graphs*, which includes Kagome, checkerboard, and pyrochlore structures, all exhibit flatbands at energy $E = 2t$, where t is the nearest-neighbor hopping amplitude. This construction was exploited by Mielke [22] to obtain ferromagnetic ground states in the presence of a Hubbard term. In each of these cases, the hoppings conspire to yield an extensive number of degenerate localized modes. Such flatband models often exhibit band touching due to additional modes from the toroidal homotopy generators [22]. A perfectly flat band can also result from interaction-induced self-energy renormalization [6]. For FCIs, nonzero Chern number [23] C as well as band flatness are desired [24], though a band with $C \neq 0$ and finite-range hoppings cannot be perfectly flat [25]. Numerical evidence indicates that this also appears true for bands with nontrivial $\mathbb{Z}_2$ topological invariants [26,27], although this result is not yet rigorously established.

In this work, we devise a systematic approach for efficiently flattening an electronic band with a given class of hopping terms. While any band may be trivially flattened via band projection, i.e., by replacing $\varepsilon_n(\boldsymbol{k})\,|\,n,\boldsymbol{k}\,\rangle\langle\,n,\boldsymbol{k}\,|$ with $|\,n,\boldsymbol{k}\,\rangle\langle\,n,\boldsymbol{k}\,|$, this maneuver comes at the cost of introducing nonlocal hoppings in real space. Our aim here is to optimize band flatness for models with physical hoppings, which are constrained by locality. This is achieved by deforming a given Hamiltonian toward one with a maximal *imaginary gap* (IG). With the help of Rouché's theorem from complex analysis, this problem can be reduced to one involving the analysis of a polynomial in a single variable. To illustrate our approach, we specialize to two-band FCIs and show how nontrivial band topology constrains the size of the IG, and thus the optimal band flatness. As a byproduct, our mathematical approach also enables the visualization of the topological index as a certain winding number, in analogy to Volovik's interpretation of the Chern number as a winding of the Green's function in complex momentum space [28].

II. FLATBANDS AND THE IMAGINARY GAP

Suppose we want to flatten the mth band of a given N-band Hamiltonian $H(\boldsymbol{k})$ with eigenvalues $\{\varepsilon_j(\boldsymbol{k})\}$. We can do so by adding a diagonal term $-\varepsilon_m(\boldsymbol{k})\,\mathbb{I}_{N\times N}$ to $H(\boldsymbol{k})$, so that [29]

$$H'(\boldsymbol{k}) = H(\boldsymbol{k}) - \varepsilon_m(\boldsymbol{k})\,\mathbb{I} \tag{1}$$

has eigenvalues $\{\varepsilon_1 - \varepsilon_m, \ldots, 0, \ldots, \varepsilon_N - \varepsilon_m\}$. To make $H'(\boldsymbol{k})$ physically realistic, we perform a real-space truncation $H'(\boldsymbol{k}) \to \tilde{H}(\boldsymbol{k})$ such that $\tilde{H}(\boldsymbol{k})$ involves only hoppings which

*calvin-lee@ihpc.a-star.edu.sg

connect unit cells separated by distances $|\boldsymbol{R}| \leqslant \Lambda$, where $\boldsymbol{R}$ is a direct lattice vector and Λ is a predefined hopping range. The mth band now acquires a finite bandwidth, as this truncation sacrifices perfect flatness for the sake of finite-range hopping.

We assume that there are no generic band crossings [30]. An appropriate dimensionless measure of the flatness of the mth band is then the ratio Δ_m/W_m of the minimal band gap,

$$\Delta_m = \min\{\varepsilon_m(\boldsymbol{k}) - \varepsilon_{m-1}(\boldsymbol{k}), \varepsilon_{m+1}(\boldsymbol{k}) - \varepsilon_m(\boldsymbol{k})\}, \quad (2)$$

across neighboring bands divided by the bandwidth $W_m = \max\|\varepsilon_m(\boldsymbol{k}) - \varepsilon_m(\boldsymbol{k}')\|_{\boldsymbol{k},\boldsymbol{k}'}$. While this depends on more information than provided by the dispersion $\varepsilon_m(\boldsymbol{k})$ alone, we find, for a wide variety of models studied, that the flatness is well approximated by

$$f = \sum_{R>0} \varepsilon(\boldsymbol{R}) \Big/ \sum_{R \geqslant \Lambda} \varepsilon(\boldsymbol{R}), \quad (3)$$

where $\varepsilon(\boldsymbol{R}) = \int_{\hat{\Omega}} \frac{d^d k}{(2\pi)^d}\, \varepsilon(\boldsymbol{k})\, e^{i\boldsymbol{k}\cdot\boldsymbol{R}}$ is the Fourier transform of the dispersion $\varepsilon(\boldsymbol{k})$ (dropping the band index m), integrated over the first Brillouin zone $\hat{\Omega}$. The numerator in Eq. (3) sets an overall energy scale roughly proportional to the typical band gap [31]. Since the bandwidth arises from the finite truncation range, it should scale approximately as the denominator.

As is well known from classical Fourier analysis [32], Fourier coefficients generically decay exponentially at an asymptotic rate given by the so-called imaginary gap (IG). The concept of the IG is employed in computing decay properties in subjects ranging from semiconductor surface science to statistical systems and quantum entanglement [33–40]. An imaginary gap g_μ can be defined for each component k_μ of the wave vector as follows. Consider the Hamiltonian $H(k_\mu)$ as a function of complex $k_\mu = \mathrm{Re}k_\mu + i\,\mathrm{Im}k_\mu$, with all other wave-vector components real and fixed. Its energy manifold consists of N Riemann sheets which represent the N bands $\varepsilon_n(k_\mu)$. The sheets do not touch at physical (real) wave vectors ($\mathrm{Im}k_\mu = 0$) where $H(k_\mu)$ is gapped, but one or more intersections $\varepsilon_m(k_\mu) = \varepsilon_{m\pm1}(k_\mu)$ always exist at complex values of k_μ, which are known as ramification or branch points [41] (see Fig. 1). The imaginary gap g_μ^m for the mth band is given by the magnitude of $\mathrm{Im}k_\mu$ minimized over all ramification points and over all other real components of the wave vector. Further minimizing over all directions, one obtains the overall IG, $g^m = \min(g_1^m, \ldots, g_d^m)$. The IG g^m is positive and unaffected by energy rescaling.

The Fourier transform of a given band's dispersion scales like $\varepsilon(R) \sim e^{-gR}$ in one dimension. This generalizes to

$$\varepsilon(\boldsymbol{R}) \sim \prod_{\mu=1}^{d} e^{-g_\mu |R_\mu|} \quad (4)$$

in higher dimensions, as derived in Appendix A, yielding a flatness parameter

$$f \sim \sum_{R>0} e^{-g_\mu |R_\mu|} \Big/ \sum_{R>\Lambda} e^{-g_\mu |R_\mu|} \sim e^{\boldsymbol{g}\cdot\boldsymbol{\Lambda}} > e^{g\|\boldsymbol{\Lambda}\|}, \quad (5)$$

where Λ_μ sets the maximal hopping range along the direction of elementary reciprocal lattice vector $\boldsymbol{a}_\mu$, and $\|\boldsymbol{\Lambda}\| = \sum_\mu \Lambda_\mu$ is the Manhattan distance [42]. When $g\,\|\boldsymbol{\Lambda}\|$ is small, the inequality in Eq. (5) is far from sharp, and we expect $\ln f \approx g(\|\boldsymbol{\Lambda}\| + r)$, where $0 < r < 1$ is a nonuniversal constant depending on $\boldsymbol{\Lambda}$ and the g_μ.

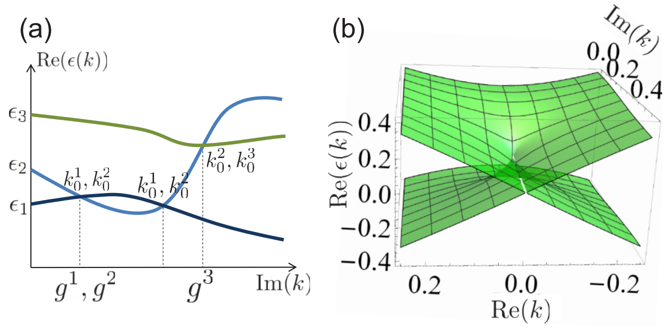

FIG. 1. (a) Illustration of the band structure of a gapped Hamiltonian in the direction of imaginary momentum. The mth band touches another band at complex $k^{(m)}$s, with the imaginary gap (IG) $g^m = \min(\mathrm{Im}k^{(m)})$. (b) Plot of $\mathrm{Re}\varepsilon_{1,2}(k)$ for the Dirac model $H(k) = \vec{d}(k)\cdot\vec{\sigma}$, with $\vec{d}(k) = (\sin k, 1+m-\cos k, 0)$ and $m = 0.3$. The physical band gap at $\mathrm{Im}k = 0$ (back of the graph) is $2m$. The two bands, which are Riemann sheets in complex momentum space, intersect (and hence are gapless) beyond the branch point at $\mathrm{Im}k \sim g \approx 0.2624$, where $H(k)$ becomes nonanalytic.

The essential insight from Eq. (5) is that a *maximization* of the IG g leads to an *exponential optimization* of the flatness ratio f. Crucially, Eq. (5) extrapolates well down to small $\|\boldsymbol{\Lambda}\|$ despite being rigorously true only for large $\|\boldsymbol{\Lambda}\|$. This is empirically evidenced in Fig. 2, which shows a high correlation between $\ln f$ and g for a variety of popular FCI

Model	$D0.2$	$D0.4$	Dwave	$D1$	CB	HC	$D5$	$D20$
g	0.18	0.33	0.79	0.88	1.01	1.21	1.39	2.94
f	1.62	3.01	6.8	5.82	26	60	37	500

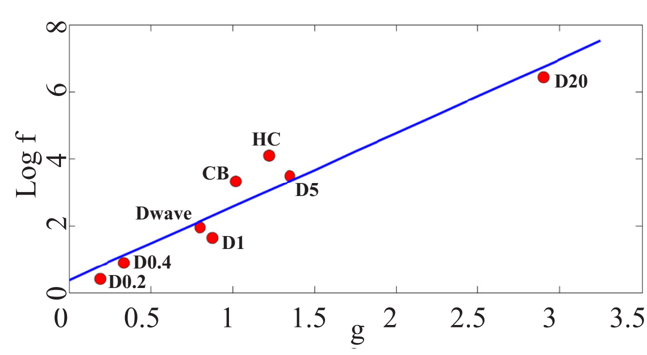

FIG. 2. Imaginary gaps g and flatness ratios f for different two-dimensional models flattened through Eq. (1) and truncated to up to NNN hoppings ($\|\boldsymbol{\Lambda}\| = 2$). Dm refers to the Dirac model [46] with mass m, Dwave to a $C = 2$ model [45], and CB and HC to the checkerboard and honeycomb FCI models, respectively [16,43]. $\ln f$ exhibits a strong correlation with g. The linear regression coefficient of 2.22 agrees well with $\|\boldsymbol{\Lambda}\| = 2$, with a comparably small nonuniversal error of $r = 0.11$. The largest IGs g are attained by the topologically trivial $m = 5$, 20 Dirac models, whereas HC shows the greatest $f \approx 60$ among all $C \neq 0$ models considered.

as well as topologically trivial models [16,43–45] with $\mathbf{\Lambda} = (1,1)$ ($\|\mathbf{\Lambda}\| = 2$), i.e., when the above truncation procedure leaves only the nearest- and next-nearest-neighbor (NN and NNN) hoppings. The value of f for preoptimized flatband models, such as the checkerboard (CB) and honeycomb (HC) models [16,43], remains nearly unchanged after the flattening by Eq. (1).

In Fig. 2, the largest f was found for topologically trivial models. This is consistent with the fact that a model with $C \neq 0$ and finite hopping range can never be completely flat. This was proven in Ref. [25] via K theory, where it was shown that the band projectors of such models must be Laurent polynomials with finite order in $z_\mu \equiv e^{ik_\mu}$. Consequently, complex singularities must be present which, in our context, imply inevitable truncation effects resulting in a nonzero bandwidth. The converse is more subtle: A perfectly flat band with $f = 0$ ($g = \infty$) can still be topologically nontrivial ($C \neq 0$) if the hoppings are not truncated. Examples include lattice models with Gaussian hoppings in a magnetic field [47], which are inspired by parent Hamiltonians [48–50] for the chiral spin liquid. Another subtlety is that chiral edge states, which are usually associated with a nontrivial Chern number, can occur in Floquet systems with flatbands [51,52].

III. ANALYTICAL OPTIMIZATION OF THE IMAGINARY GAP

The imaginary gap (IG) g of $H(\boldsymbol{k})$ provides a good lower bound of the flatness ratio $f \gtrsim e^{g\|\mathbf{\Lambda}\|}$ for the bands of the flattened $\tilde{H}(\boldsymbol{k})$. The next step is to compute g efficiently. We want to generate a local $N \times N$ model $\tilde{H}(\boldsymbol{k})$ with an almost flat band and hopping terms satisfying $\tilde{H}(\boldsymbol{R}) = 0$ for $|R_\mu| > \Lambda_\mu$. This can be done via Eq. (1), followed by a truncation of the resulting $H(\boldsymbol{k}) \to \tilde{H}(\boldsymbol{k})$. Expressed in terms of the $z_\mu = e^{ik_\mu}$, we have $\tilde{H}_{ij}(z) = [\tilde{H}_{ji}(z)]^*$, with each $\tilde{H}_{ij}(z)$ a Laurent polynomial in each of the z_μ with powers ranging from $z_\mu^{-\Lambda_\mu}$ to $z_\mu^{+\Lambda_\mu}$; note that $z_\mu^{-1} = z_\mu^*$ for z on the unit circle, which is the boundary of the analytic continuation region. The energy eigenvalues $\varepsilon_n(z)$ are roots of the characteristic polynomial,

$$P(\varepsilon; z) = \det[\varepsilon\, \mathbb{I}_{N\times N} - \tilde{H}(z)]. \tag{6}$$

The energy manifold is singular at the roots of the discriminant,

$$D(z) = \prod_{m<n}^{N} [\varepsilon_m(z) - \varepsilon_n(z)]^2, \tag{7}$$

which is defined for any N. As shown in Appendix B, $D(z)$ can be expressed [53] in terms of the coefficients $p_l(z)$ of $P(\varepsilon; z) = \sum_{l=0}^{N} p_l(z)\, \varepsilon^{N-l}$, with $p_0 \equiv 1$. For $\boldsymbol{k} \in \mathbb{R}^d$, the coefficients are real because they are symmetric polynomials in the eigenenergies: $p_1(z) = -\sum_j \varepsilon_j(z)$, $p_2(z) = \sum_{j<l} \varepsilon_j(z)\, \varepsilon_l(z)$, etc. From Eq. (6), each $p_l(z)$ is a polynomial in each z_μ with negative degree $-l\Lambda_\mu$ and positive degree $+l\Lambda_\mu$. In what follows, it suffices to know that $D(z)$ is itself a multinomial of maximal degrees $\pm M_\mu = \pm N(N-1)\Lambda_\mu$ in each z_μ. For local $N = 2$ band models which can be written as $\tilde{H}(z) = \vec{d}(z) \cdot \vec{\sigma}$ [54], the discriminant reduces to the familiar expression $D(z) = \sum_{j=1}^{3} d_j^2(z)$.

We are now ready to optimize the IG. We first compute, in each direction μ, the IG $g_\mu = \min |\mathrm{Re} \ln \xi_\mu|$, where ξ_μ is a root of $D(\ldots, z_\mu, \ldots)$, with all $z_{\mu'}$ for $\mu' \neq \mu$ considered as parameters with respect to which the minimization is performed. Expressed as a Laurent polynomial, the discriminant may be written as

$$D(z) = \sum_{n=-M}^{M} D_n z^n, \tag{8}$$

where $D_{-n} = D_n^*$, and where we have dropped the direction index μ. We now analytically continue to [55] $|z| \neq 1$. The Hermiticity of $\tilde{H}$ guarantees that if $D(z) = 0$, then $D(1/z^*) = 0$, and hence *exactly* M of the $2M$ roots of the analytic function $z^M D(z)$ will lie within the unit circle $|z| = 1$. The IG is then determined by the root lying closest to $|z| = 1$.

The task of finding this root is greatly facilitated by Rouché's theorem [32], which states that if $|f(z)| > |h(z) - f(z)|$ on a closed contour $\mathcal{C}$, then $f(z)$ and $h(z)$ have the same number of zeros within $\mathcal{C}$. To understand this intuitively, consider a man at $f(z)$ walking a dog at $h(z)$ near a tree. Let $\arg(z)$ denote the winding around the tree. If the dog's leash is shorter than the minimal distance of the man from the tree, the dog and the man must encircle the tree the same number of times.

Now let $f(z) = D_0 z^M$ and $h(z) = z^M D(z)$, with the contour $\mathcal{C}$ being the circle $|z| = \Delta$. Clearly, $f(z)$ has an M-fold degenerate root at $z = 0$ and no others. Since $|\sum_{n\neq 0} D_n z^n| < \sum_{n\neq 0} |D_n|\, \Delta^{M+n}$ on $\mathcal{C}$, where the sums are over $n \in \{\pm 1, \ldots, \pm M\}$, Rouché's theorem then guarantees that if $|D_0|\Delta^M > \sum_{n\neq 0} |D_n|\, \Delta^{M+n}$, the function $h(z) = z^M D(z)$ also has M roots within $\mathcal{C}$. Since the right-hand side of the inequality increases without bound for $\Delta \gg 1$, we conclude that $g_\mu > -\ln \Delta$, where Δ is the smallest positive root of

$$F(\Delta) \equiv \sum_{n=1}^{M} |D_n|(\Delta^{M+n} + \Delta^{M-n}) - |D_0|\, \Delta^M. \tag{9}$$

The problem of finding a lower bound for the IG has been reduced to the simpler problem of solving a real polynomial equation, $F(\Delta) = 0$. Essentially, we sacrificed an exact determination of g_μ to settle for a lower bound, and at the same time avoided the necessary step of finding the arguments of the roots of $h(z)$. We shall see below that this lower bound is already sufficient in providing an estimate of f.

Equation (9) can be solved numerically, and in certain cases analytically via the substitution

$$U = \Delta + \Delta^{-1}. \tag{10}$$

An optimally flat model may be obtained by varying $H(\boldsymbol{k})$ until the root $\Delta > 0$ in Eq. (9) is minimized. If $\Delta < 1$ is maintained throughout the minimization, no branch point ever touches the unit circle, i.e., the physical gap never closes, and we remain in the same topological class.

IV. TWO-BAND CHERN MODELS

Many of the important flatband models such as the honeycomb, checkerboard, and Dirac models contain only $N = 2$

bands and NN hoppings ($\|\mathbf{\Lambda}\|=1$). Their discriminants are, at most, of quadratic ($M=2$) degree, and can be readily studied and optimized analytically. We write the truncated Hamiltonian as $\tilde{H}(z)=\vec{d}(z)\cdot\vec{\sigma}$, where $z=e^{ik}$ for a given momentum component. The $\vec{d}$ vector takes the form

$$\vec{d}=2(\vec{w}\cos k-\vec{v}\sin k)+\vec{\beta}, \tag{11}$$

where $\vec{w}$, $\vec{v}$, and $\vec{\beta}$ are real three-component vectors that depend parametrically on the other momenta. With $\vec{\alpha}\equiv\vec{w}+i\vec{v}$, we can rewrite $\vec{d}$ as $\vec{d}=\vec{\alpha}\,z+\vec{\alpha}^*z^{-1}+\vec{\beta}$. The coefficients in the discriminant may now be given: $D_0=2\vec{\alpha}\cdot\vec{\alpha}^*+\vec{\beta}\cdot\vec{\beta}$, $D_1=2\vec{\alpha}\cdot\vec{\beta}$, and $D_2=\vec{\alpha}\cdot\vec{\alpha}$. Substituting these expressions in Eq. (9) and letting $U=\Delta+\Delta^{-1}$, we obtain

$$U=\sqrt{\left|\frac{D_1}{2D_2}\right|^2+\left|\frac{D_0}{D_2}\right|}-\left|\frac{D_1}{2D_2}\right|. \tag{12}$$

Since $\Delta\leqslant 1$, we choose the root $\Delta=\frac{1}{2}(U-\sqrt{U^2-4})$, yielding a lower bound for the overall flatness ratio f in the direction μ:

$$f>\min_{\mu}\left\{\tfrac{1}{2}U_\mu+\sqrt{\tfrac{1}{4}U_\mu^2-1}\right\}, \tag{13}$$

which is monotonically increasing in U_μ, where Δ_μ and U_μ are the *minimal* U and *maximal* Δ in direction μ, optimized over the wave-vector components in all other directions. Note that the flatness ratio f increases with decreasing $|D_2|$ when U is sufficiently large. In terms of the original three vectors,

$$\begin{aligned}|D_0|&=2|\vec{w}\,|^2+2|\vec{v}\,|^2+|\vec{\beta}\,|^2,\\ |D_1|&=2\sqrt{(\vec{w}\cdot\vec{\beta})^2+(\vec{v}\cdot\vec{\beta})^2},\\ |D_2|&=\sqrt{(|\vec{w}\,|^2-|\vec{v}\,|^2)^2+4(\vec{w}\cdot\vec{v})^2},\end{aligned} \tag{14}$$

which are rotationally invariant, consistent with the basis independence of $\tilde{H}(z)$. Note also from Eq. (12) that f is unaffected by an overall rescaling of $\vec{w}$, $\vec{v}$, and $\vec{\beta}$. To maximize U, and hence f, we want $|D_{1,2}|\ll|D_0|$.

Topological constraint on flatness

1. $D_2=0$ cases

The parametrization in terms of $\vec{w}$, $\vec{v}$, and $\vec{\beta}$ suggests a geometric interpretation. Various FCI models belong to the simplest case of $D_2=0$, where $|\vec{w}\,|=|\vec{v}\,|$ and $\vec{w}\cdot\vec{v}=0$; for $D_2\neq 0$ cases, see the next section. From Eq. (12),

$$U=\left|\frac{D_0}{D_1}\right|=\frac{|\vec{w}\,|^2+|\vec{v}\,|^2+\frac{1}{2}|\vec{\beta}\,|^2}{|\vec{w}\,||\vec{\beta}_\parallel|}, \tag{15}$$

where $\vec{\beta}_\parallel$ is the component of $\vec{\beta}$ in the plane spanned by $\vec{w}$ and $\vec{v}$: $\vec{\beta}\equiv\vec{\beta}_\parallel+\vec{\beta}_\perp$. To optimize flatness, $\vec{\beta}$ must avoid the largest possible torus of constant U, defined by

$$|\vec{\beta}_\perp|^2+(|\vec{\beta}_\parallel|-U\,|\vec{w}\,|)^2=|\vec{w}\,|^2(U^2-4). \tag{16}$$

For large U, its approximate inner and outer radii are $2U^{-1}|\vec{w}\,|$ and $2U|\vec{w}\,|$. Thus, $\vec{\beta}$ should either have a small magnitude inside the "donut hole" or a large one outside the torus.

Consider optimizing f in the x direction for a two-dimensional model, so that $\vec{\beta}=\vec{\beta}(k_y)$ traces out a loop as k_y varies over a period. To remain in the same topological class, $\vec{\beta}$ must not pass through any point where the gap closes, i.e., where $U_x=2$, which occurs when $|\vec{\beta}|=|2\vec{w}|$. This is just the ring of radius $|2\vec{w}|$ in the plane spanned by $\vec{v}$ and $\vec{w}$, centered at its origin (Fig. 3). Configurations belonging to the same topological class thus are those that can be reached without intersecting this nodal ring, i.e., those $\vec{\beta}$ loops have the same *winding number* around the ring. To maximize $\min(U_x)$, we can either increase the size of the loop $\vec{\beta}(k_y)$ or shift it far away from the origin. A large loop, however, entails large coefficients of the terms in k_y, which will lead to small U_y when the same procedure is applied to the k_y direction. Hence a model with minimal f in both directions should have loops $\vec{\beta}(k_x)$ and $\vec{\beta}(k_y)$ of radii of the same order of magnitude as $|\vec{w}\,|=|\vec{v}\,|$.

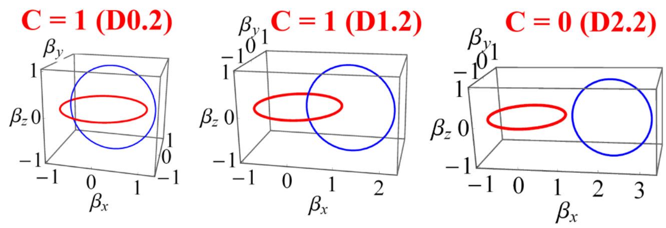

FIG. 3. Nodal ring $U=U_x=2$ representing gap closure [red, Eq. (12)], and $\vec{\beta}$ loop [blue, Eq. (11)] representing the $\vec{d}$ vector of Eq. (17) for $m=0.2$, 1.2, and 2.2. The linking number between the ring and the loop is 1 in the $m<2$ regime where $C=1$, and zero otherwise. The two loops are furthest separated at $m=1$, which also makes that the case with the highest flatness ratio [see Eq. (16)].

It is now clear how topology constrains f: In the topologically trivial case, $\vec{\beta}$ need not wind around the nodal ring, yet can still entail arbitrarily large $\min(U_x)$ and $\min(U_y)$ by being far from the ring. In contrast, nontrivial topology requires that the $\vec{\beta}$ loop winds around the nodal ring, constraining its size and position.

2. Example: 2D Dirac model

Consider the two-dimensional (2D) Dirac Hamiltonian

$$\tilde{H}(\boldsymbol{k})=\sin k_x\sigma^x+\sin k_y\sigma^y+(m+\cos k_x+\cos k_y)\sigma^z, \tag{17}$$

which is Eq. (11) with $k\to k_x$, $\vec{w}=(0,0,\frac{1}{2}),\vec{v}=(-\frac{1}{2},0,0)$, and $\vec{\beta}=(0,\sin k_y,m+\cos k_y)$. We have $|D_2|=0$, $|D_1|=m+\cos k_y$, and $|D_0|=2+2m\cos k_y+m^2$. Equation (17) is symmetric in k_x and k_y, so $g_x=g_y$, and we only need to consider one direction, k_x. The ratio that determines the band flatness is $U_x=|D_0/D_1|$. It attains extremal values when $\cos k_y=\pm 1$, where

$$U_x=\left|\frac{D_0}{D_1}\right|=\left|m\pm 1+\frac{1}{m\pm 1}\right|. \tag{18}$$

We then obtain the flatness ratio $f\geqslant\Delta_x^{-2}=\Delta_y^{-2}$ by choosing the larger of the solutions to $\Delta_x=\Delta=\frac{1}{2}(U-\sqrt{U^2-4})$. The optimal flatness ratio bound is obtained at $m=\sqrt{2}$, where $f=3+\sqrt{8}\approx 5.82$. In this case, the bound set by Rouché's theorem is saturated. A numerical computation from $\tilde{H}(\boldsymbol{k})$ gives an actual flatness ratio of $f\approx 6$, which is close to our lower bound. One can verify that in this case, the

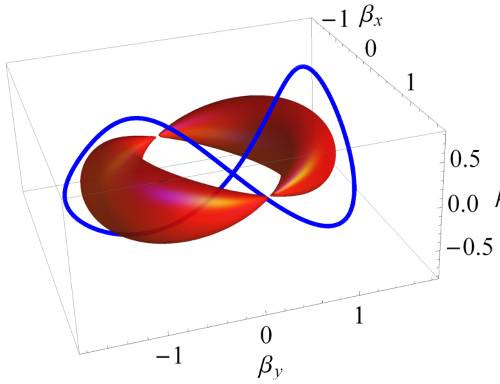

FIG. 4. An illustration of the nodal surface (red) and $\vec{\beta}$ loop (blue) for the general case $D_2 \neq 0$, with constant $|v| = 1.05\,|w|$ and $\vec{w}\cdot\vec{v} = 0.05\,|\vec{w}||\vec{v}|$. Shown is $\vec{\beta}$ with linking number 2.

inequality in Rouché's theorem is saturated for *all* values of m. Geometrically, we see that $\vec{\beta}$ describes a circle of radius unity: $(\beta_y - m)^2 + \beta_x^2 = 1$. As shown in Fig. 3, it has a linking number of 1 with the nodal circle $\beta_x^2 + \beta_y^2 = 1$ for $0 < |m| < 2$, i.e., $C = \pm 1$.

3. General cases with nonzero D_2

We now discuss the geometric picture for general two-dimensional two-band models with D_2 not necessarily zero. From the general expression of U in Eq. (9) of the main text, we find that the nodal points (where $U = 2$) occur at $|D_0| = \frac{1}{2}|D_1| + \frac{1}{2}|D_2|$. As shown in Fig. 4, the nodal ring in general broadens to become two bean-shaped surfaces that intersect at two points. In general, their exact shape will also depend on the other momentum parameters.

Most importantly, this general case is topologically identical to the $D_2 = 0$ case. The Chern number remains the winding number of $\vec{\beta}$ around the nodal region, which still has the same topology as the ring, except that there are two additional topologically trivial regions inside each of the bean-shaped surfaces. $\vec{\beta}$ loops inside them are limited to small values of U, and are of limited usefulness to the search of flatband models with large f.

V. CONCLUSION

We have restated the band flattening problem for a truncated Hamiltonian $\tilde{H}(\boldsymbol{k})$ with finite-range hoppings in terms of the optimization of the *imaginary gap*, which is the smallest imaginary component of the wave vector for which the Hamiltonian $\tilde{H}(\boldsymbol{k})$ is singular. Appealing to Rouché's theorem, this optimization is further reduced to an analysis of a finite-order polynomial, and finally to a vector geometry problem. Our approach provides geometric insight into how a nonzero Chern number imposes a finite bandwidth for short-range hopping models. It also offers a constructive approach to optimizing the band flatness of short-range hopping models.

ACKNOWLEDGMENTS

R.T. thanks J. Budich and M. Maksymenko for discussions. R.T. is funded by the European Research Council through ERC-StG-TOPOLECTRICS-336012 and by DFG-SFB 1170.

APPENDIX A: DECAY PROPERTIES OF THE EIGENENERGIES $\varepsilon(k_x,k_y)$ IN REAL SPACE AND THE IMAGINARY GAP

We provide a derivation that the scaling behavior of real-space hoppings $\varepsilon(\boldsymbol{R})$ is given by $\prod_{\mu=1}^{d} e^{-g_\mu |R_\mu|}$, where g_μ is the imaginary gap for $\boldsymbol{k}$ parallel to the elementary reciprocal lattice vector $\boldsymbol{b}_\mu$, with other components of $\boldsymbol{k}$ held fixed. This result forms the basis of Eq. (3) of the main text. For ease of notation, we specialize to the case of two dimensions, $\boldsymbol{R} = (X,Y)$. First, we clarify how the analytic continuation is performed. The energy of a particular band $\varepsilon(k_x,k_y)$ is a function of two variables, which we analytically continue to the complex plane one at a time, while regarding the other as a parameter, i.e., $\varepsilon(k_x,k_y) \to \varepsilon(z,k_y)$ with $z = e^{ik_x}$.

The Fourier decay rate $g_x(k_y)$ can be found by finding the location of the singularity of $\varepsilon(z,k_y)$ closest to the unit circle $|z| = 1$. Analyzing $\varepsilon(k_x,z)$ with $z \equiv e^{ik_y}$ yields $g_y(k_x)$. We now find the asymptotic bound on $\varepsilon(X,Y)$. First, we Fourier transform over k_x,

$$\begin{aligned}\varepsilon(X,Y) &= \int_{\hat{\Omega}} \frac{d^2k}{(2\pi)^2}\, \varepsilon(k_x,k_y)\, e^{i(k_x X + k_y Y)} \\ &= \int \frac{dk_y}{2\pi}\, \varepsilon(X,k_y)\, e^{ik_y Y} \\ &\sim \int \frac{dk_y}{2\pi}\, e^{-g_x(k_y)|X|}\, e^{i\theta(X,k_y)}\, e^{ik_y Y}, \qquad \text{(A1)}\end{aligned}$$

where we have invoked $|\varepsilon(X,k_y)| \sim e^{-g_x(k_y)|X|}$ [32]. The quantity $\theta(X,k_y)$ represents an unknown phase that turns out to be irrelevant. Next we do the k_y Fourier transform. We obtain a simple bound upon expanding about the minimum g_x of $g_x(k_y)$,

$$\begin{aligned}\varepsilon(X,Y) &\sim \left| \int \frac{dk_y}{2\pi}\, e^{-g_x(k_y)|X|}\, e^{i\theta(X,k_y)}\, e^{ik_y Y} \right| \\ &\leqslant \int \frac{dk_y}{2\pi}\, |e^{-g_x(k_y)|X|}| \\ &= \int \frac{dk_y}{2\pi}\, e^{-g_x|X|}\, e^{-g_x''(k_y - k_y^0)^2|X|/2 + \cdots} \\ &\approx (2\pi|X|\,g_x'')^{-1/2} e^{-g_x|X|} \sim e^{-g_x|X|}, \qquad \text{(A2)}\end{aligned}$$

where k_y^0 is the value of k_y where $g_x(k_y) = g_x$ is minimized, and g_x'' is the curvature at that point. The above approximation is justified in the limit of large $|X|$, where higher-order terms in $(k_y - k^0)$ are rapidly suppressed. As such, only contributions from $g_x(k_y) = g_x$ and a small neighborhood around it are non-negligible. Note that we have replaced the periodic integral over k_y with an infinite integral above, so the former will not be strictly correct in the limit of constant $g_x(k_y)$. Still, the result $\varepsilon(X,Y) \sim e^{-g_x|X|}$ holds in that case.

If we repeat the above derivations starting from the partial Fourier transform $\varepsilon(k_x,Y)$ instead, we obtain an analogous bound involving g_y. Combining these results, we obtain

$$\varepsilon(X,Y) \sim e^{-g_x|X| - g_y|Y|} < e^{-g\|\boldsymbol{R}\|}. \qquad \text{(A3)}$$

Equation (3) of the main text predicts a flatness ratio of $f \sim e^{g\|\mathbf{A}\|}$ after a real-space truncation of $\varepsilon(X,Y)$ that retains only terms within $|X| \leqslant \Lambda_x$ and $|Y| \leqslant \Lambda_y$. This ratio depends crucially on Eq. (A3), which is exact only in the asymptotic limit of large Λ. In practice, however, it provides excellent agreement with numerical results even for $\parallel \mathbf{\Lambda} \parallel = ||(1,1)|| = 2$, as shown explicitly in Fig. 2 of the main text, and in the example on the Dirac model (also see main text). As mentioned, g_μ only rigorously controls the real-space decay rate asymptotically. Furthermore, the derivation leading to Eq. (A3) also contains large $|\boldsymbol{R}|$ approximations. There may also be certain peculiarities in the shape of ε that suppress certain Fourier components, e.g., the case of the D-wave model, which has a poor overlap with the first harmonics $\cos k_x$ and $\cos k_y$. These will lead to an anomalous decay not captured in the asymptotics. When g is small, the next smallest truncated terms will not be much smaller than the leading truncated terms, being only suppressed by a factor e^{-g}, and the decay rate should in fact lie between $g \parallel \mathbf{\Lambda} \parallel$ and $g(\parallel \mathbf{\Lambda} \parallel +1)$.

APPENDIX B: MORE ON THE DISCRIMINANT

1. Explicit form

The discriminant of a polynomial

$$P(\varepsilon; z) = \sum_{l=0}^{N} p_l(z)\, \varepsilon^{N-l}, \tag{B1}$$

with $p_0 = 1$, can be expressed in terms of the resultant of $P(\varepsilon)$ and its derivative $P'(\varepsilon)$ (with z suppressed). The resultant is proportional to the determinant of the $(2N-1) \times (2N-1)$ Sylvester matrix shown below, where the first $N-1$ rows consist of the coefficients of $P(\varepsilon)$ and the next N rows consist of the coefficients of $P'(\varepsilon)$. Written out explicitly, the discriminant is equal to $(-1)^{N(N-1)/2}/p_N$ times the determinant of the Sylvester matrix,

$$\begin{bmatrix} p_N & p_{N-1} & p_{N-2} & \cdots & p_1 & p_0 & 0\ldots & \ldots & 0 \\ 0 & p_N & p_{N-1} & p_{N-2} & \cdots & p_1 & p_0 & 0\ldots & 0 \\ \vdots & & & & & & & & \vdots \\ 0 & \ldots & 0 & p_N & p_{N-1} & p_{N-2} & \ldots & p_1 & p_0 \\ N\,p_N & (N-1)\,p_{N-1} & (N-2)\,p_{N-2} & \ldots & 1\,p_1 & 0 & \ldots & \ldots & 0 \\ 0 & N\,p_N & (N-1)\,p_{N-1} & (N-2)\,p_{N-2} & \ldots & 1\,p_1 & 0 & \ldots & 0 \\ \vdots & & & & & & & & \vdots \\ 0 & 0 & \ldots & 0 & N\,p_N & (N-1)\,p_{N-1} & (N-2)\,p_{N-2} & \ldots & 1\,p_1 \end{bmatrix}. \tag{B2}$$

Since p_l is of maximal degree $l\Lambda_\mu$ in z_μ, the discriminant as shown above must be of maximal degree,

$$\deg D(z) = 2\Lambda_\mu(1 + 2 + \cdots + N) = N(N-1)\Lambda_\mu. \tag{B3}$$

More generally, the resultant of two polynomials disappears whenever the two polynomials have a common root.

2. Alternatives to the discriminant

When $N > 2$, the roots of the discriminant gives us all the possible branch points, even those not associated with the mth energy sheet that we desire to be almost flat. Consequently, the flatness of the desired band in $\tilde{H}(\boldsymbol{k})$ may be underestimated. To remedy this, we may alternatively *define* g_μ to include only the roots of $(\varepsilon_m - \varepsilon_{m+1})^2(\varepsilon_m - \varepsilon_{m-1})^2$. However, this procedure may be more complicated to perform analytically, involving the explicit solution of the degree N characteristic polynomial. An analytic solution may not even exist for $N \geqslant 5$ due to the Abel-Ruffini theorem [32], although this is not too constraining since most interesting flatband models in the literature contain no more than $N = 4$ bands.

[1] H. Tasaki, From Nagaoka's ferromagnetism to flat-band ferromagnetism and beyond: An introduction to ferromagnetism in the Hubbard model, Prog. Theor. Phys. **99**, 489 (1998).

[2] Z. Liu, F. Liu, and Y.-S. Wu, Exotic electronic states in the world of flatbands: From theory to material, Chin. Phys. B **23**, 077308 (2014).

[3] M. Garnica, D. Stradi, S. Barja, F. Calleja, C. Díaz, M. Alcamí, N. Martín, A. L. V. de Parga, F. Martín, and R. Miranda, Long-range magnetic order in a purely organic 2D layer adsorbed on epitaxial graphene, Nat. Phys. **9**, 368 (2013).

[4] H. N. Kono and Y. Kuramoto, Variational Monte Carlo study of flat band ferromagnetism–Application to $CeRh_3B_2$–, J. Phys. Soc. Jpn. **75**, 084706 (2006).

[5] Y. Suwa, R. Arita, K. Kuroki, and H. Aoki, Spin-density-functional study of the organic polymer dimethylaminopyrrole: A realization of the organic periodic Anderson model, Phys. Rev. B **82**, 235127 (2010).

[6] Z. Gulácsi, A. Kampf, and D. Vollhardt, Route to Ferromagnetism in Organic Polymers, Phys. Rev. Lett. **105**, 266403 (2010).

[7] N. Masumoto, N. Y. Kim, T. Byrnes, K. Kusudo, A. Löffler, S. Höfling, A. Forchel, and Y. Yamamoto, Exciton–polariton condensates with flat bands in a two-dimensional kagome lattice, New J. Phys. **14**, 065002 (2012).
[8] F. Baboux, L. Ge, T. Jacqmin, M. Biondi, E. Galopin, A. Lemaître, L. L. Gratiet, I. Sagnes, S. Schmidt, H. E. Türeci *et al.*, Bosonic Condensation and Disorder-Induced Localization in a Flat Band, Phys. Rev. Lett. **116**, 066402 (2016).
[9] L. Van Hove, The occurrence of singularities in the elastic frequency distribution of a crystal, Phys. Rev. **89**, 1189 (1953).
[10] H. Tasaki, Ferromagnetism in the Hubbard Models with Degenerate Single-Electron Ground States, Phys. Rev. Lett. **69**, 1608 (1992).
[11] M. Maksymenko, A. Honecker, R. Moessner, J. Richter, and O. Derzhko, Flat-Band Ferromagnetism as a Pauli-Correlated Percolation Problem, Phys. Rev. Lett. **109**, 096404 (2012).
[12] S. Miyahara, S. Kusuta, and N. Furukawa, BCS theory on a flat band lattice, Physica C: Superconductivity **460**, 1145 (2007).
[13] G. Karakonstantakis, L. Liu, R. Thomale, and S. A. Kivelson, Correlations and renormalization of the electron-phonon coupling in the honeycomb Hubbard ladder and superconductivity in polyacene, Phys. Rev. B **88**, 224512 (2013).
[14] C. Wu, D. Bergman, L. Balents, and S. Das Sarma, Flat Bands and Wigner Crystallization in the Honeycomb Optical Lattice, Phys. Rev. Lett. **99**, 070401 (2007).
[15] E. Tang, J.-W. Mei, and X.-G. Wen, High-Temperature Fractional Quantum Hall States, Phys. Rev. Lett. **106**, 236802 (2011).
[16] K. Sun, Z. Gu, H. Katsura, and S. Das Sarma, Nearly Flatbands with Nontrivial Topology, Phys. Rev. Lett. **106**, 236803 (2011).
[17] T. Neupert, L. Santos, C. Chamon, and C. Mudry, Fractional Quantum Hall States at Zero Magnetic Field, Phys. Rev. Lett. **106**, 236804 (2011).
[18] N. Regnault and B. A. Bernevig, Fractional Chern Insulator, Phys. Rev. X **1**, 021014 (2011).
[19] S. A. Parameswaran, R. Roy, and S. L. Sondhi, Fractional quantum Hall physics in topological flat bands, C. R. Phys. **14**, 816 (2013).
[20] M. Claassen, C.-H. Lee, R. Thomale, X.-L. Qi, and T. P. Devereaux, Position-Momentum Duality and Fractional Quantum Hall Effect in Chern Insulators, Phys. Rev. Lett. **114**, 236802 (2015).
[21] O. Derzhko, J. Richter, and M. Maksymenko, Strongly correlated flat-band systems: The route from Heisenberg spins to Hubbard electrons, Int. J. Mod. Phys. B **29**, 1530007 (2015).
[22] A. Mielke, Ferromagnetic ground states for the Hubbard model on line graphs, J. Phys. A: Math. Gen. **24**, L73 (1991).
[23] S.-Y. Lee, J.-H. Park, G. Go, and J. H. Han, Arbitrary Chern number generation in the three-band model from momentum space, J. Phys. Soc. Jpn. **84**, 064005 (2015).
[24] Note that FCIs were recently proposed for interaction scales larger than the band gap [56], as well as in a topologically trivial band [57]. However, nearly flat Chern bands with large band gaps are still likely to be the most suited for stabilizing an FCI.
[25] L. Chen, T. Mazaheri, A. Seidel, and X. Tang, The impossibility of exactly flat non-trivial Chern bands in strictly local periodic tight binding models, J. Phys. A: Math. Theor. **47**, 152001 (2014).
[26] V. Ozoliņš, R. Lai, R. Caflisch, and S. Osher, Compressed modes for variational problems in mathematics and physics, Proc. Natl. Acad. Sci. USA **110**, 18368 (2013).
[27] J. C. Budich, J. Eisert, E. J. Bergholtz, S. Diehl, and P. Zoller, Search for localized Wannier functions of topological band structures via compressed sensing, Phys. Rev. B **90**, 115110 (2014).
[28] G. E. Volovik, *The Universe in a Helium Droplet* (Oxford University Press, Oxford, 2003).
[29] This simple replacement avoids dealing directly with the band projectors which, being operators, require more mathematical care.
[30] This is guaranteed by the Wigner–von Neumann theorem when the codimension for accidental degeneracies is greater than the physical dimension of space, as occurs, i.e., in two-dimensional systems with broken time-reversal symmetry.
[31] Equation (3) may not hold when certain real-space terms conspire to cancel in a special way. However, such cases are the exception, as evidenced by the wide variety of models in Fig. 2 that adhere fundamentally to Eq. (3). See also Appendix A.
[32] S. Lang, *Complex Analysis* (Springer, New York, 2013), Vol. 103.
[33] W. Kohn, Analytic properties of bloch waves and wannier functions, Phys. Rev. **115**, 809 (1959).
[34] P. N. First, J. A. Stroscio, R. A. Dragoset, D. T. Pierce, and R. J. Celotta, Metallicity and Gap States in Tunneling to Fe Clusters in GaAs(110), Phys. Rev. Lett. **63**, 1416 (1989).
[35] W. Mönch, Empirical tight-binding calculation of the branch-point energy of the continuum of interface-induced gap states, J. App. Phys. **80**, 5076 (1996).
[36] L. He and D. Vanderbilt, Exponential Decay Properties of Wannier Functions and Related Quantities, Phys. Rev. Lett. **86**, 5341 (2001).
[37] T. Thonhauser and D. Vanderbilt, Insulator/Chern-insulator transition in the Haldane model, Phys. Rev. B **74**, 235111 (2006).
[38] W. Mönch, On the band-structure lineup at Schottky contacts and semiconductor heterostructures, Mater. Sci. Sem. Proc. **28**, 2 (2014).
[39] C. H. Lee and A. Lucas, Simple model for multiple-choice collective decision making, Phys. Rev. E **90**, 052804 (2014).
[40] C. H. Lee and P. Ye, Free-fermion entanglement spectrum through Wannier interpolation, Phys. Rev. B **91**, 085119 (2015).
[41] This occurs at the roots of the discriminant (see Appendix B), which always exist from the fundamental theorem of algebra.
[42] The decay rates from the different directions contribute additively to the total decay exponent.
[43] Y.-F. Wang, Z.-C. Gu, C.-D. Gong, and D. N. Sheng, Fractional Quantum Hall Effect of Hard-Core Bosons in Topological Flat Bands, Phys. Rev. Lett. **107**, 146803 (2011).
[44] C. H. Lee, R. Thomale, and X.-L. Qi, Pseudopotential formalism for fractional Chern insulators, Phys. Rev. B **88**, 035101 (2013).
[45] C. H. Lee and X.-L. Qi, Lattice construction of pseudopotential Hamiltonians for fractional Chern insulators, Phys. Rev. B **90**, 085103 (2014).
[46] X.-L. Qi, T. L. Hughes, and S.-C. Zhang, Topological field theory of time-reversal invariant insulators, Phys. Rev. B **78**, 195424 (2008).

[47] E. Kapit and E. Mueller, Exact Parent Hamiltonian for the Quantum Hall States in a Lattice, Phys. Rev. Lett. **105**, 215303 (2010).
[48] D. F. Schroeter, E. Kapit, R. Thomale, and M. Greiter, Spin Hamiltonian for which the Chiral Spin Liquid is the Exact Ground State, Phys. Rev. Lett. **99**, 097202 (2007).
[49] R. Thomale, E. Kapit, D. F. Schroeter, and M. Greiter, Parent Hamiltonian for the chiral spin liquid, Phys. Rev. B **80**, 104406 (2009).
[50] E. I. Rashba, L. E. Zhukov, and A. L. Efros, Orthogonal localized wave functions of an electron in a magnetic field, Phys. Rev. B **55**, 5306 (1997).
[51] M. S. Rudner, N. H. Lindner, E. Berg, and M. Levin, Anomalous Edge States and the Bulk-Edge Correspondence for Periodically Driven Two-Dimensional Systems, Phys. Rev. X **3**, 031005 (2013).
[52] I. C. Fulga and M. Maksymenko, Scattering matrix invariants of Floquet topological insulators, Phys. Rev. B **93**, 075405 (2016).
[53] B. P. Brooks, The coefficients of the characteristic polynomial in terms of the eigenvalues and the elements of an n× n matrix, Appl. Math. Lett. **19**, 511 (2006).
[54] Throughout, we use boldface to denote vectors in position/momentum space, and arrows to denote vectors in internal (spin) space.
[55] The analytic continuation of a function onto a domain is uniquely defined by its boundary values. Otherwise, the difference between two different continuations will be trivially zero on the boundary, but nontrivial within the domain. Here, $z_j^* = z_j^{-1}$ on the boundary $|z_j| = 1$, which uniquely defines the analytic continuation shown.
[56] S. Kourtis, T. Neupert, C. Chamon, and C. Mudry, Fractional Chern Insulators with Strong Interactions that Far Exceed Band Gaps, Phys. Rev. Lett. **112**, 126806 (2014).
[57] S. H. Simon, F. Harper, and N. Read, Fractional Chern insulators in band with zero Berry curvature, Phys. Rev. B **92**, 195104 (2015).